Full Paper

www.molinf.com

molecular informatics

DOI: 10.1002/minf.201900111

In Silico Analysis of FDA Drugs as P2X4 Modulators for the Treatment of Alcohol Use Disorder

Francisco Reyes-Espinosa,[a] María G. Nieto-Pescador,[b] Virgilio Bocanegra-García,[a] Eduardo Lozano-Guzmán,[b] and Gildardo Rivera*[a]

Abstract: Recent studies have shown the potential application of ivermectins in the treatment of alcohol use disorder (AUD). Ivermectin is a positive allosteric modulator (PAM) of P2X4R and this molecule exerts its action in the transmembrane region (known as the TM region) of trimeric channel structure (the pocket formed by Asp331, Met336, Trp46, Trp50, and Tyr42). The aim of this study is to identify FDA drugs with potential PAM properties, by exploring the P2X4Rs from four organisms (*Danio rerio*, *Mus musculus*, *Rattus norvegicus*, and *Homo sapiens*). The *in silico* study consists of carrying out the molecular docking of 1656 FDA-approved drugs on the structure of P2X4R, using the commercially available compounds from the ZINC[15] database for virtual screening. To strengthen the reliability of the results, two docking protocols were used involving the use of two programs, Autodock 4.2 and Autodock Vina. Nine FDA drugs with potential PAM properties were identified. In addition, eight molecules with potential negative allosteric modulator (NAM) action, and 13 molecules with potential allosteric modulator (AM) action were identified. The FDA drugs identified in this study with PAM, NAM, and AM action, shared in the P2X4Rs of the four organisms, can provide a guideline to proceed with research concerning new drugs for the study and treatment of AUD.

Keywords: P2X4 receptor · drug repositioning · allosteric modulators · molecular modeling · molecular docking · virtual screening

1 Introduction

According to the National Institute on Alcohol Abuse and Alcoholism (NIAA), alcohol use disorder (AUD) is a chronic relapsing brain disease characterized by compulsive alcohol use and loss of control over alcohol. It is estimated that in the United States 16 million people have this disease. AUD causes important diverse negative health effects on organs and tissues. It also represents a social problem for the family, friends, and society. Currently, disulfiram, naltrexone, and acamprosate are the only FDA drugs approved for the treatment of AUD. Acamprosate was the last drug approved to treat alcoholism, although other drugs in clinical research could be repositioned (varenicline, gabapentin, topiramate, ondansentron, nalmefene, and baclofen) as new options for pharmacological treatment (consulted on National Institute on Alcohol Abuse and Alcoholism (NIAAA). Available online: https://www.niaaa.nih.gov (accessed 1 March 2019)).[1]

In recent years, P2X4 receptors (P2X4Rs) emerged as a valid target for AUD. Ivermectin (IVM) has been described as a potential modulator of this receptor.[2,3,4] P2X4Rs belong to the purinergic ion channel family (P2XRs) and are activated by extracellular ATP; P2X4Rs are most widely distributed in the central nervous system.[5] P2X4R modulates major neurotransmitter systems and regulates alcohol-induced responses in microglia.[6]

Even though ivermectins are proposed to have multiple central nervous system objectives, Huynh *et al.* (2019) gave evidence that most of their anti-alcohol effects come from the interaction with P2X4Rs. Therefore, this type of compound could be repositioned in the future to develop novel AUD pharmacotherapies.

Native P2X4 channels are sensitive to ethanol at intoxicating concentrations and ethanol can also allosterically inhibit the function of the receptor, through the interaction of ethanol with the transmembrane domain of P2X4R.[6] Asatryan *et al.* (2010)[3] presented a study that revealed a pocket located in the TM region (a pocket formed by Asp331, Met336, Trp46, and Trp50) that may play a role in the actions of ethanol and IVM. Latapiat *et al.* in 2017, provided evidence of the participation of zinc and IVM as allosteric modulators of P2X4Rs, acting at independent allosteric modulator sites.[4] These are relevant findings in the treatment of AUD. Therefore, the objective of this work was the repositioning of FDA drugs from the ZINC[15]

[a] *F. Reyes-Espinosa, V. Bocanegra-García, G. Rivera*
Laboratorio de Biotecnología Farmacéutica, Centro de Biotecnología Genómica, Instituto Politécnico Nacional, 88710, Reynosa, México
E-mail: gildardors@hotmail.com
[b] *M. G. Nieto-Pescador, E. Lozano-Guzmán*
Facultad de Ciencias Químicas, Universidad Juárez del Estado de Durango, 34120, Durango, México
Phone: +52 (899)9243627 Ext. 87758
E-mail: mgnieto@ujed.mx

Supporting information for this article is available on the WWW under https://doi.org/10.1002/minf.201900111

database (http://zinc15.docking.org/)[7,8] as P2X4R modulators for the treatment of AUD by virtual screening using the following steps: (a) construction of molecular models of P2X4Rs orthologues from four organisms (zebrafish, mouse, rat, and human), (b) performance of a docking analysis of drug compounds approved by the FDA on the constructed P2X4Rs models, and (c) identification of the structures with allosteric modulator action of P2X4Rs shared in *D. rerio, M. musculus, R. norvegicus* and *H. sapiens*. These four organisms, because of their orthologues P2X4Rs, have been widely used as study models -recently analyzed and widely discussed by Huynh *et al*, 2019 about the relationship between P2X4Rs and ethanol behaviour and how they are using P2X4Rs as a drug-development as novel AUD medications-, and there is a lot of information on their structural characterization – mainly for zebrafish – well as experimental evidence of their function, in particular, only in two systems, mouse and rat. To perform the virtual screening, two docking programs were used, AutoDock 4.2 and AutoDock Vina. Thus, we performed a computational study modeling the potential allosteric inhibition of P2X4Rs orthologues.

2 Materials and Methods

2.1 Homology Modeling

The P2X4 receptor sequences of the four organisms were retrieved from the UniProt Knowledgebase (Available online: http://www.uniprot.org/help/uniprotkb – accessed 1 February, 2019)[9,10] with the following identification codes: Q99571 (*Homo sapiens*, human), P51577 (*Rattus norvegicus*, rat), Q9JJX6 (*Mus musculus*, mouse) and Q6NYR1 (*Danio rerio*, zebrafish). The molecular models of P2X4 receptors were constructed by homology modeling of protein structures with SWISS-MODEL (Available online: https://swissmodel.expasy.org/ – accessed 1 February 2019)[11,12] operating in user-template mode, using the PDB 4DW1[13] and 3I5D[14] as a template to build the open and closed trimeric structures; both structures were downloaded from RCSB PDB (Available online: www.rcsb.org – accessed 1 February 2019).[15,16]

2.2 Molecules used in Virtual Screening

A total of 1657 molecular structures contained in the catalogues of FDA-approved drugs only were obtained from the ZINC[15] database (Available online: http://zinc15.docking.org/ – accessed 1 December 2018).[7,8] In addition, three structures were downloaded from ZINC[15]: ivermectin (IVM, ZINC238808778), abamectin (ABM, ZINC245224134) and selamectin (SEL, ZINC169677006). All molecules were saved in mol2 format.

2.3 Molecular Docking

In order to perform molecular docking, the molecular models of P2X4 receptors were prepared with Dock Prep tools of the UCSF Chimera program.[17] P2X4 receptor and molecule structures were saved in PDBQT format using AutoDockTools 1.5.6[11] according to the standard protocol. Docking parameter files were developed using AutoDockTools and Docking was performed using Autodock4.2[18] and AutoDock Vina.[19] For each open and closed protein structure, a GridBox was built with a dimension set of X = 60, Y = 60 and Z = 60 pts, with a spacing of 0.375 Å, and their respective center coordinates were, for open protein structure, X = −36.600, Y = −21.335 and Z = 55.799, and for closed protein structure, X = −35.58, Y = −32.415 and Z = 21.467; To perform AutoDock Vina, a GridBox was built with a similar size (a dimension set of X = 22.5, Y = 22.5 and Z =

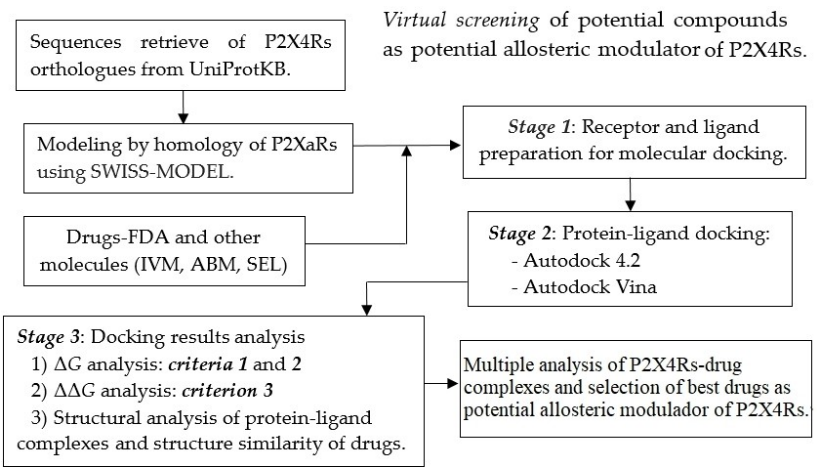

Figure 1. Protocol used to perform the virtual screening of the *in silico* study of the P2X4Rs-drug complex.

22.5 pts with a spacing of 1.0 Å) and their respective center coordinates were the same, already indicated on both protein structures, open and closed, respectively. Affinity maps were generated using AutoGrid4 and the atom types were extracted by screening all PDBQT ligand files. The protein-ligand interactions on the binding sites were analyzed using Protein-Ligand Interaction Profiler, PLIP server (Available online: http://plip.biotec.tu-dresden.de/plip-web – accessed 1 March 2019).[20,21] All programs were installed on a Linux Mint 17.3 operating system implemented with a 3.4 GHz Intel Core i7 processor and 23.5 GB RAM.

3 Results and Discussion

3.1 Computational Protocol

The computational protocol implemented (Materials and Methods) consisted of three stages (Figure 1): (a) Receptor and ligand preparation, which included homology modeling of protein structures using SWISS-MODEL,[11,12] (b) Molecular docking performed with Autodock 4.2[18] and AutoDock Vina,[19] and (c) Characterization of interactions in P2X4Rs-drug (protein-ligand) complexes executed with the PLIP program.[20,21]

3.2 Homology Modeling of P2X4Rs Orthologues

The trimeric structures of P2X4Rs models of *D. rerio, M. musculus, R. norvegicus*, and *H. sapiens* organisms were constructed according to a previously presented methodology.[22] Typical results of homology modeling (open and closed models) are shown in Figure 2. The

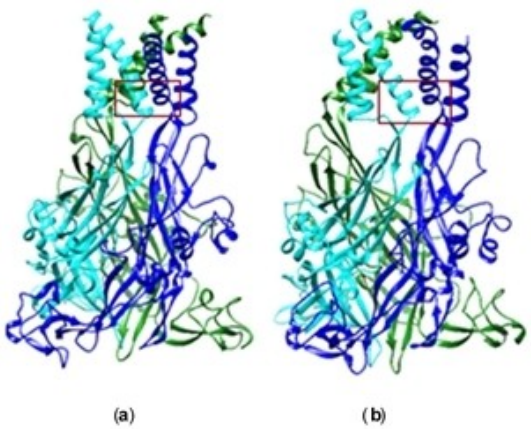

Figure 2. 3D P2X4Rs, axial view of the trimeric structure. Open (a) and closed models (a): blue, green and cyan chain represents the respective monomeric structure. The box in red indicates the location of the binding site of IVM.

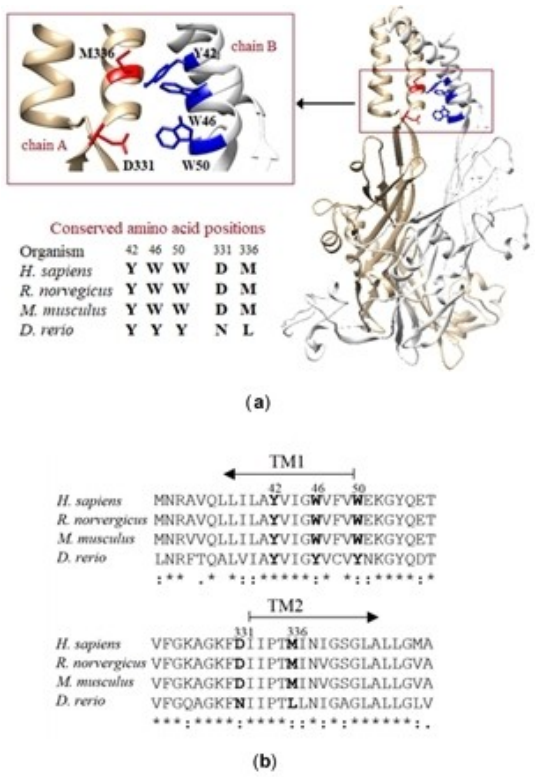

Figure 3. Molecular P2X4Rs model based on dimeric structure to illustrate conserved amino acid positions in transmembrane (TM) region (a). Sequence alignment between TM region of P2X4R orthologues (b).

quality of the model registered in the Homology Modeling Report of SWISS-MODEL,[15,16] referred to as energy analysis of the qualitative model (GMQE and QMEAN score) are shown in Table 1. The QMEAN scoring function assesses the global and per-residue model quality.[12] The sequence alignment of the four organisms involved is presented in Figure A1 (Appendix A). Score as multiple alignment 3D results from the built models with respect to the templates are presented in Figure A2 (Appendix A). The score obtained from the 3D- structural alignment of the models built with respect to the structures used as a template are shown in Figure A2; this analysis is referred to as Cα-alignment.

The region where the docking study was performed is located on the transmembrane (TM) structure (Figure 3a). The trimeric structure of P2X4Rs comprises six TM helices, two for each subunit (Figure 2); differences in structural properties were detected in each (sub)pockets (Figure A3, Appendix A), analysis performed with DoGSiteScore program.[23] The TM region studied is highly conserved (see Figure 3 a–b) in the four structures analyzed (Figure 3b). Crystallography studies reported by Kawate *et al.* in 2009 revealed that the TM helices are oriented approximately

Table 1. Model building report obtained of the trimeric structure of P2X4Rs.[9,10]

Organism	ID codes	Template: PDB 4DW1* GMQE	QMEAN	SI	Template: PDB 3I5D* GMQE	QMEAN	SI
H. sapiens	Q99571	0.81	−1.83	0.61	0.82	−1.93	0.62
R. norvegicus	P51577	0.81	−1.34	0.62	0.82	−1.93	0.63
M. musculus	Q9JJX6	0.81	−1.68	0.61	0.82	−2.09	0.61
D. rerio	Q6NYR1	0.99	−1.07	0.99	0.99	−1.52	0.98

GMQE, Global Model Quality Estimation (values from 0 to 1); QMAN, Energy Analysis of the Qualitative Model; *, structure retrieved from RCSB PDB;[15,16] SI, Sequence identity.

antiparallel to one another and are angled nearly 45° from the normal membrane.[14]

Research concerning the study of actions of ethanol and IVM have focused on the pocket formed by Asp331, Met336, Trp46, Trp50, and Tyr42. Previous research indicates that position 331 (Asp331) and 336 (Met336) in the TM2 segment is critical for ethanol modulation of P2X4Rs.[24] The anthelmintic medication, IVM, positively modulates P2X4Rs and is believed to act in the same region as ethanol.[3] Recently, several research groups have contributed preclinical evidence that demonstrates the potential use of avermectins (IVM, SEL, ABM, and moxidectin – MOX) in the treatment of AUD.[25–28]

3.3 Molecular Docking Results

A total of 1657 FDA-approved drugs were evaluated on P2X4Rs structures of *D. rerio, M. musculus, R. norvegicus*, and *H. sapiens*. The systems under study comprise two types of trimeric structures, P2X4R models in open and closed state (Figure 4). The potential allosteric inhibition of P2X4R by FDA drugs can be analyzed in two aspects, the first is a quantitative analysis based on binding energy (ΔG_b), and the second, a qualitative analysis based on interactions recorded in the P2X4R-drug complex. Both model structures (open and closed state) were used to perform the virtual screening by the two docking programs, Autodock 4.2[19] and AutoDock Vina.[19]

In order to perform a comparison between the ΔG_b predicted by molecular docking programs, we proceeded to calculate the relative binding energy ($\Delta\Delta G$), which is a thermodynamic parameter that allows the analysis of the ΔG_b difference present in the systems under study (ΔG_b^s) in relation to a reference system (ΔG_b^r). $\Delta\Delta G$ is defined as $\Delta\Delta G = \Delta G_b^s - \Delta G_b^r$, where the superscript s and r both refer to the system in comparison. Therefore, to identify potential allosteric inhibitor compounds of P2X4Rs, the docking results analysis were performed applying the following three criteria:

Criterion 1. This consists of selecting only one system, which is used as a reference to make an arbitrarily assigned cut of $\Delta G_b^{\pounds} < -8.5$ Kcal/mol. The P2X4R rat evaluated with the Autodock 4.2 program was the system selected as a cutoff reference (see Figure 5 c). The result of applying criterion 1 was obtained with 37 drugs (see Figure 5, symbols in black).

Criterion 2. The second is the consistency in ΔG_b recorded in both programs, Autodock 4.2 (see Figure 6 a–d) and Autodock Vina (see Figure 6 e–h), to register a lower ΔG_b. This was based on the following arbitrary expression: $\Delta\Delta G^{\lambda} > -8.5$ Kcal/mol, where $\Delta\Delta G^{\lambda} = (((\Delta G_b^{open})^2 + (\Delta G_b^{closed})^2) * 0.5)^{0.5}$. Then, applying criterion 2 ($\Delta\Delta G^{\lambda} > -8.5$ Kcal/mol), 30 drugs were obtained in a graph (ΔG_b^{open} vs ΔG_b^{closed} scores) of docking results which are shown in Figure 6.

Criterion 3. Grouping the results according to the $\Delta\Delta G^{\S}$ value, where $\Delta\Delta G^{\S} = \Delta G_b^{open} - \Delta G_b^{closed}$. Three categories were obtained (see Figure 6) shown as series A, favourable to closed structure ($\Delta\Delta G^{\S} > 0.5$ Kcal/mol), series B, with good affinity but indeterminate (-0.5 Kcal/mol $< \Delta\Delta G^{\S} <$ 0.5 Kcal/mol), and series C, favourable to open structure ($\Delta\Delta G^{\S} < -0.5$ Kcal/mol). $\Delta\Delta G^{\S}$ value is related to potential action as an allosteric modulator (AM) of P2X4Rs (data shown in Table 2).

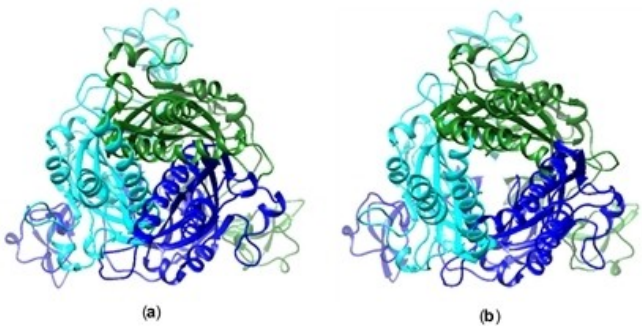

Figure 4. 3D P2X4Rs, top view of the trimeric structure. (a) Typical molecular models open; (b) Typical molecular models closed; blue, green and cyan chain represents the respective monomeric structure.

3.4 Structural Similarity Analysis

In order to find structurally similar compounds (unlike identifying compounds sharing a specific substructure) in the 30 drugs that were identified as a result of applying criterion 2, the FragFp descriptor was calculated using the DataWarrior program.[29] The result of the similarity analysis is presented in Figure 7. The presence of a group that shares structural similarity with IVM is notable, and in this group, we also find the ABM and SEL molecules. The respective 2D structures of the molecules recorded in this analysis are presented in Table B1 (Appendix B).

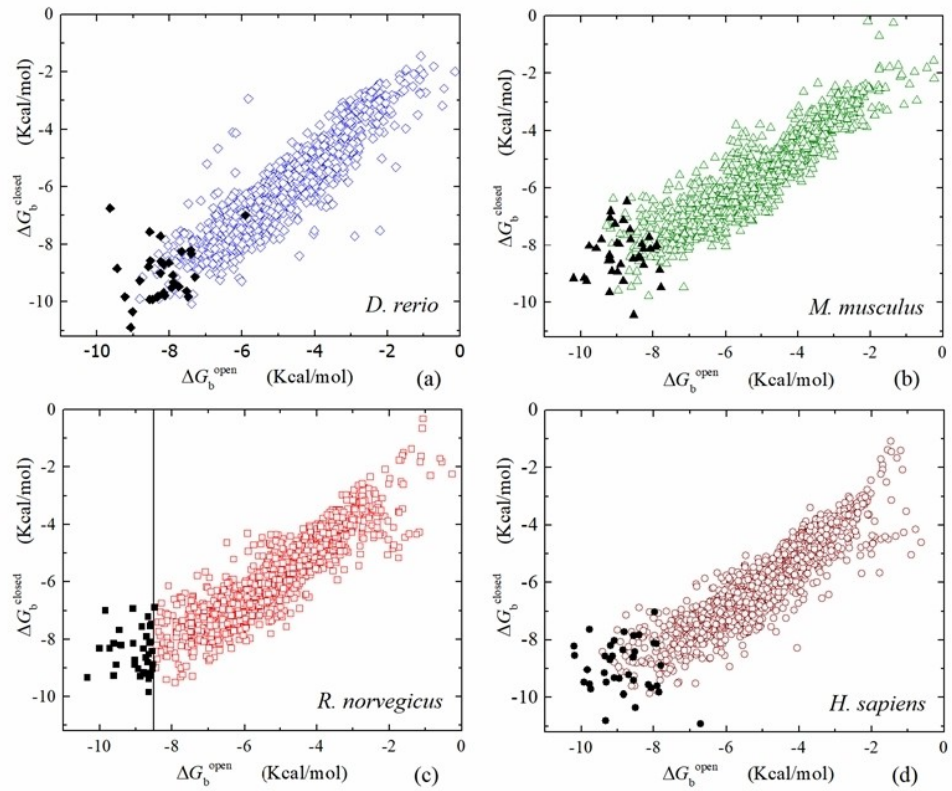

Figure 5. Docking results of 1657 drugs evaluated on P2X4Rs shown as ΔG_b^{open} vs ΔG_b^{closed} scores. ΔG_b was predicted with the Autodock 4.2 program. The system selected as a cutoff reference was P2X4Rs of rat (c), 37 drugs as a result of applying criterion 1: symbols in black $\Delta G_b^{£}$ value < -8.5 Kcal/mol. Docking results to zebrafish (a), mouse (b) and human (d) P2X4Rs.

3.5 Interaction Profile in P2X4Rs in Complex with Evaluated Molecules

Previous studies conducted with the rat P2X4R model in which molecular dynamics was used provided evidence that the IVM molecule was stable in that position.[4,25] The 30 drugs evaluated have cyclic structures (see Table B1); consequently, the interactions recorded involve interactions with the residues Asp331, Met336, Trp46, Trp50, and Tyr42 (data not shown).

There is no consistency in the selected drugs (properties such as size – Table 3 – and functional groups – Figure 5a); consequently, there is no interaction profile that provides more information to the study. We consider that the interactions obtained in molecular docking could be verified with molecular dynamics (which is not the purpose of the present study) or proceed with *in vitro* evaluations to test the allosteric modulator action of P2X4Rs.

3.6 Allosteric Modulators of P2X4Rs

For purposes of analyzing the results of this study, we refer to series A, molecules as allosteric modulators (AMs), due to their potential non-specific potential or blocking action. We refer to series B and series C as negative allosteric modulators (NAMs) and positive allosteric modulators (PAMs), respectively. PAMs are also known as allosteric enhancers or potentiators because they induce an amplification of the effect of the primary ligand. Conversely, NAMs reduce the effect of the primary ligand. In this context, we understand the ligand as the molecule with the capacity to favour open conformation of the P2X4Rs channel.

The present study allows us to identify AMs of P2X4Rs. In the first instance, as a result of applying criterion 3, we identified molecules with desirable properties. This was achieved with the previous evaluation of criterion 1, in which molecules with desirable properties were selected in rat P2X4Rs (a model of which there is a lot of information in the literature), and the evaluation of criterion 2, in which there is a priority for human model P2X4Rs (the central model of the present study). Criterion 3 allows categorization into three types of P2X4Rs modulators (AMs, NAMs, and PAMs), being of particular interest the PAMs due to the fact that IVM is a PAM of P2X4R.[2,3]

The reliability of the results obtained is based on the reproducibility obtained from two protocols for molecular docking. This involved the use of the Autodock 4.2 program and Autodock Vina. The reproducibility of the results (see Table 2) is notorious in the magnitude of the $\Delta\Delta G^{§}$ (where

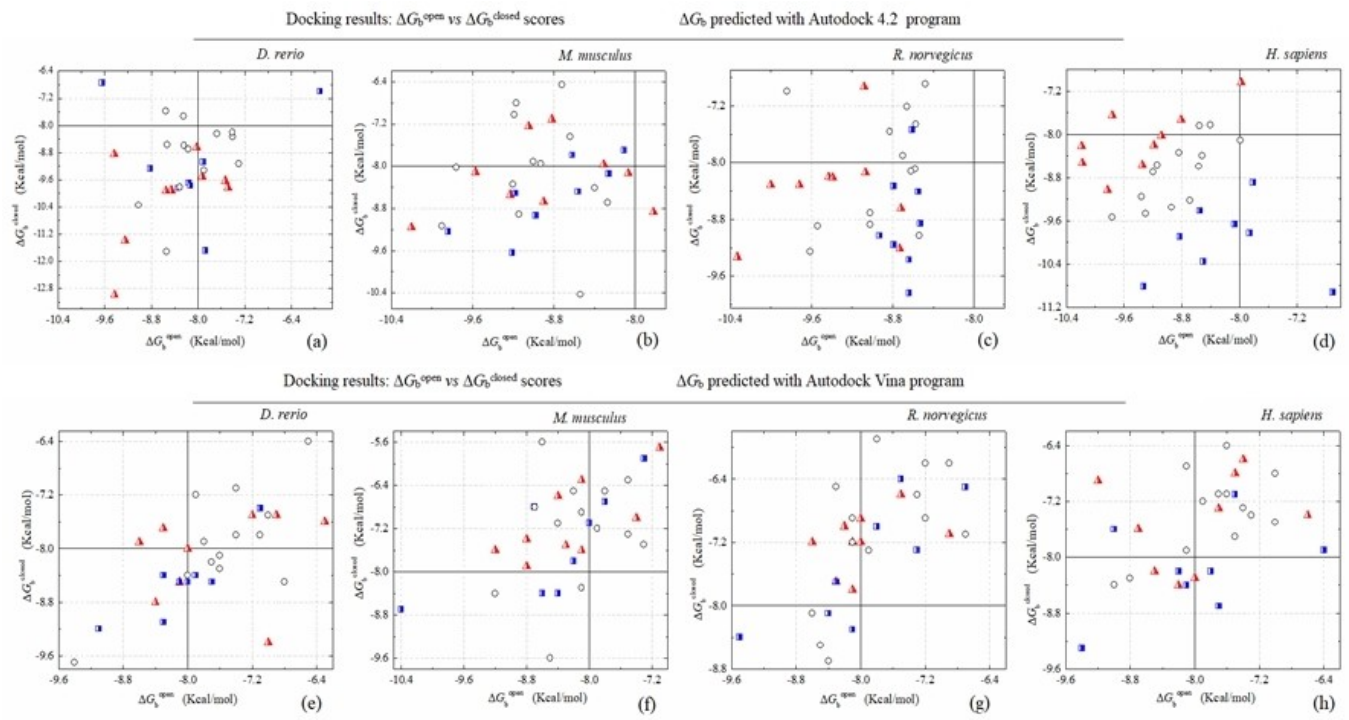

Figure 6. Docking results (ΔG_b^{open} vs ΔG_b^{closed} scores); 30 drugs were identified as a result of applying criterion 2 ($\Delta\Delta G^{\S}$ value > -8.5 Kcal/mol). Graphs a–d show ΔG_b predicted with Autodock 4.2 program and Graphs e-h show ΔG_b predicted with Autodock Vina program. Grouping the results according to criterion 3, the docking results are shown as squares in blue – series A – (good affinity but indeterminate, -0.5 Kcal/mol $< \Delta\Delta G^{\S} < 0.5$ Kcal/mol), circles in black – series B – (favourable to closed structure, $\Delta\Delta G^{\S} > 0.5$ Kcal/mol), and triangles in red – series C – (favourable to open structure, $\Delta\Delta G^{\S}$ value < -0.5 Kcal/mol). ΔΔG§ ($\Delta\Delta G^{\S} = \Delta G_b^{open} - \Delta G_b^{closed}$), data values are shown in Table 2.

Figure 7. Structural similarity (FragFp descriptor) of data from Table 2. IVM structure (ZINC238808778).

$\Delta\Delta G^{\S} = \Delta G_b^{open} - \Delta G_b^{closed}$) registered in series B (b1-b8 drugs) and series C (c1–c9 drugs). The cases where there is no agreement between the magnitudes of $\Delta\Delta G^{\S}$ are grouped in series A (a1–a13 drugs).

Table 3 shows examples of approved drugs identified *in silico* in the present study. General information about these approved drugs is presented in Table S1 (*Supplementary Materials*).

3.7 Perspectives of P2X4R in the Treatment of Others Diseases

Others research groups has been reported relevant potential applications of P2X4R in the treatment of different diseases, for example, Zabala *et al.* (2018)[30] investigated the potential of P2X4R as a drug target in the effect of IVM in multiple sclerosis. Experimental autoimmune encephalomyelitis clinical symptoms were exacerbated by P2X4R blockage and ameliorated by P2X4R potentiation with the allosteric modulator, IVM.[30] Pharmacological activation of the P2X4R expressed by brain microglia has been studied as a pharmacological target for demyelinating diseases.[31]

Abdelrahman *et al.* in 2017, highlighted the link between upregulation of the P2X4 receptor and microglial

Table 2. Consistency of results of ΔG_b and $\Delta\Delta G^{\S}$ values obtained in docking evaluation of P2X4Rs (zebrafish, mouse, rat and human organisms) with 30 drugs were identified as result of applying criterion 2 by performing docking with Autodock 4.2 program and Autodock Vina program.

ID	ID ^{Zinc15}	$\Delta G_b{}^{Za\ \Delta\Delta G\S}$ AD4/Vina	$\Delta G_b{}^{Ms\ \Delta\Delta G\S}$ AD4/Vina	$\Delta G_b{}^{Rn\ \Delta\Delta G\S}$ AD4/Vina	$\Delta G_b{}^{Hs\ \Delta\Delta G\S}$ AD4/Vina
IVM	238808778	$-8.3^{1.3}/-7.6^{0.5}$	$-8.6^{-1.5}/-7.8$*	$-8.3^{-0.8}/-7.6^{-0.5}$	$-8.1^{0.5}/-7.8$*
ABM	122404486	$-6.8^{1.9}/-7.8$*	$-7.5^{-0.3}/-6.9$*	$-7.1^{0.3}/-7.2$*	$-7.3^{-0.4}/-7.0$*
SEL	124201874	$-8.3^{1.3}/-7.9^{0.5}$	$-8.4^{-0.7}/-8.4$*	$-7.8^{-0.7}/-7.9^{-0.8}$	$-8.4^{-0.9}/-8.1^{-0.7}$
a1	DB11575	$-8.5^{3.2}/-7.4$*	$-9.2^{-2.2}/-8.7^{-1.9}$	$-9.8^{-2.9}/-8.3^{-1.8}$	$-8.6^{-0.7}/-7.9^{-0.7}$
a2	DB01045	$-7.7^{0.6}/-7.4$*	$-9.0^{-1.1}/-8.7^{-1.9}$	$-8.6^{-0.5}/-8.1^{-0.9}$	$-8.4^{-0.6}/-7.7^{-0.6}$
a3	DB00966	$-7.9^{1.4}/-7.0^{0.5}$	-8.4*$/-8.1$*	-9.0*$/-8.6^{-0.5}$	$-9.1^{-0.6}/-7.6^{-0.5}$
a4	DB00976	-8.2*$/-7.9^{-0.7}$	$-9.2^{-2.4}/-8.1^{-1.2}$	$-8.8^{-1.3}/-7.3^{-0.7}$	$-9.2^{-0.5}/-7.6^{-1.2}$
a5	DB05109	$-8.2^{0.5}/-7.6^{0.5}$	$-8.9^{-1.0}/-7.8^{-1.3}$	$-8.5^{-1.6}/-7.8^{-1.9}$	$-8.8^{-0.5}/-7.5$*
a6	DB00872	$-9.0^{1.3}/-9.4$*	$-9.9^{-0.8}/-9.2^{-0.8}$	-9.6*$/-8.5$*	-9.8*$/-9.0^{-0.6}$
a7	DB08827	$-7.4^{0.9}/-6.8^{1.7}$	$-9.8^{-1.7}/-7.5$*	$-8.7^{-0.8}/-7.9^{-0.6}$	-9.4*$/-7.4$*
a8	DB01167	$-7.3^{1.8}/-7.6^{0.7}$	-8.3*$/-7.9^{-0.7}$	$-8.6^{-0.5}/-7.2^{-1.0}$	-8.5*$/-7.3$*
a9	DB00444	$-8.3^{1.5}/-7.1^{0.7}$	$-8.6^{-1.2}/-7.5^{-1.2}$	$-8.6^{-1.1}/-6.9^{-0.7}$	-8.6*$/-7.0$*
a10	DB00864	$-7.4^{0.8}/-7.1^{0.7}$	$-8.7^{-2.3}/-8.6^{-3.0}$	$-8.7^{-1.5}/-7.2$*	-8.0*$/-8.1^{-1.4}$
a11	DB06290	$-8.6^{-1.0}/-8.0$*	$-9.2^{-0.9}/-8.4^{-1.3}$	$-9.5^{-0.6}/-8.1^{-1.2}$	-9.3*$/-8.1$*
a12	DB00549	$-8.3^{-0.5}/-7.8$*	-9.1*$/-7.3$*	$-8.5^{0.5}/-6.7$*	-8.9*$/-7.0^{0.5}$
a13	DB00646	-8.5*$/-7.7^{0.5}$	$-8.5^{1.9}/-8.5^{1.1}$	-9.0*$/-8.4$*	$-8.7^{0.5}/-8.8^{-0.5}$
b1	DB04868	$-7.9^{1.2}/-8.3$*	-8.6*$/-8.7^{-1.9}$	-8.5*$/-8.3^{-0.6}$	$-8.6^{0.9}/-9.0^{-1.4}$
b2	DB00390	$-8.2^{1.5}/-7.9$*	-9.0*$/-8.4$*	-8.6*$/-8.1$*	$-8.8^{1.1}/-8.1$*
b3	DB13879	$-8.1^{1.7}/-7.7^{0.8}$	$-8.6^{-0.8}/-7.8^{-1.1}$	$-8.6^{-1.1}/-7.5^{-1.1}$	$-7.8^{1.1}/-7.5$*
b4	DB09158	-8.8*$/-8.3^{0.8}$	-9.2*$/-8.2$*	$-8.6^{1.2}/-7.8^{-0.8}$	$-9.3^{1.5}/-8.2$*
b5	DB09534	$-7.9^{3.8}/-9.1$*	-8.3*$/-10.4^{-1.7}$	$-8.6^{0.7}/-9.5^{-1.1}$	$-8.1^{1.6}/-9.4$*
b6	DB00762	$-8.3^{1.5}/-8.1$*	$-9.2^{-0.7}/-8.0^{-0.9}$	-8.8*$/-7.3$*	$-8.5^{1.9}/-7.7^{1.0}$
b7	DB06809	$-5.9^{1.1}/-7.1$*	-8.1*$/-7.3^{-1.4}$	$-8.8^{-0.5}/-6.7$*	$-7.9^{2.0}/-6.4^{1.5}$
b8	DB11581	$-9.6^{-2.9}/-8.0$*	$-9.8^{-0.6}/-8.6$*	-8.9*$/-8.4$*	$-6.7^{4.2}/-7.8$*
c1	DB09297	$-9.3^{2.1}/-8.6^{-0.7}$	$-10.2^{-1.0}/-8.8^{-1.4}$	$-10.3^{-1.0}/-8.1$*	$-9.8^{-2.1}/-8.2$*
c2	DB01248	$-9.4^{3.6}/-6.3^{1.3}$	$-9.1^{1.8}/-8.4^{-1.8}$	$-10.0^{-1.7}/-8.0^{-0.8}$	$-10.2^{-2.0}/-7.5^{-0.7}$
c3	DB01201	$-9.4^{-0.6}/-8.3^{-0.6}$	-8.1*$/-9.2^{-1.6}$	$-9.7^{-1.4}/-8.6^{-1.4}$	$-10.2^{-1.7}/-8.7^{-1.1}$
c4	DB00877	$-7.9^{1.6}/-8.0$*	-8.3*$/-8.1^{-0.5}$	$-9.1^{-0.9}/-8.2^{-1.2}$	$-8.8^{-1.1}/-7.7$*
c5	DB01590	$-7.5^{2.1}/-6.9^{0.6}$	$-7.8^{1.1}/-7.4$*	$-9.4^{-1.2}/-8.0^{-1.1}$	$-9.1^{-1.1}/-7.4^{-0.8}$
c6	DB00615	$-8.0^{0.6}/-8.1$*	$-9.6^{-1.5}/-8.3^{-0.8}$	$-9.4^{-1.2}/-8.1^{-0.9}$	$-9.2^{-1.0}/-8.0$*
c7	DB06772	$-7.5^{2.3}/-7.2$*	$-8.8^{-1.7}/-7.1^{-1.4}$	$-9.1^{-2.2}/-6.9$*	$-8.0^{-1.0}/-6.6^{0.8}$
c8	DB00320	$-8.5^{1.5}/-7.0^{2.4}$	$-9.2^{-0.7}/-8.1^{-1.8}$	$-8.7^{0.5}/-7.5^{-0.9}$	$-9.8^{-0.8}/-9.2^{-2.3}$
c9	DB00696	$-8.6^{1.4}/-8.4$*	-8.9*$/-8.8^{-0.9}$	-8.7*$/-8.3^{-0.6}$	$-9.4^{-0.8}/-8.5$*

Series a (good affinity but indeterminate (-0.5 Kcal/mol $< \Delta\Delta G^{\S} < 0.5$ Kcal/mol), a1–a13 drugs; series b (favourable to closed structure, $\Delta\Delta G > 0.5$ Kcal/mol), b1–b8 drugs; and series c (favourable to open structure, $\Delta\Delta G^{\S} < -0.5$ Kcal/mol), c1–c9 drugs; $\Delta\Delta G^{\S} = \Delta G_b{}^{open} - \Delta G_b{}^{closed}$; Hs, *H. sapiens*; Rn, *R. norvegicus*; Ms, *M. musculus*; Za, *D. rerio.*

activation in the neuroinflammatory mechanism, pointing out the pharmacological blockade of the receptor as a potential treatment of chronic neuropathic pain and in neuroprotection,[34,35] as well as possibly in other types of chronic pain and inflammatory pain.[6,34,36–41] Therefore, the compounds reported in this study could be analyzed as a potential option for theses diseases.

4 Conclusion

The implemented computer protocol allows the identification of molecules with desirable properties of positive allosteric modulators (PAMs) of P2X4Rs, such as ivermectin (IVM). Due to their registered energy values as potential PAMs and their low molecular weight, we suggest two drugs, dihydroergotamine, and ergotamine as AMs. The methodology implemented considers the virtual screening carried out in P2X4Rs orthologues (*H. sapiens, R. norvegicus, M. musculus* and *D. rerio* organisms); therefore, the approved drugs identified as AMs could be evaluated in rat or mouse.

Abbreviations

ABM	Abamectin
IVM	Ivermectin
P2XRs	P2X receptors
SEL	Selamectin
P2X4Rs	P2X4 receptors
CNS	Central nervous system

Table 3. Description of FDA approved drugs identified as results from the in silico study on P2X4Rs.

ID	Accession Number	*e.g.* Drug	Molecular groups	Molecular formula [C]	MW [C] (g/mol)
IVM	ZINC238808778 [A]	Ivermectin	App; Inv; App^{V}	$C_{48}H_{74}O_{14}$	875.11
ABM	ZINC245224134 [A]	Abamectin	—	$C_{48}H_{72}O_{14}$	873.09
SEL	ZINC169677006 [A]	Selamectin	—	$C_{43}H_{63}NO_{11}$	769.97
a1	DB11575 [B]	Grazoprevir	App.	$C_{38}H_{50}N_6O_9S$	766.92
a2	DB01045 [B]	Rifampicin	App.	$C_{43}H_{58}N_4O_{12}$	822.95
a3	DB00966 [B]	Telmisartan	App.; Inv.	$C_{33}H_{30}N_4O_2$	514.63
a4	DB00976 [B]	Telithromycin	App.	$C_{43}H_{65}N_5O_{10}$	812.02
a5	DB05109 [B]	Trabectedin	App.; Inv.	$C_{39}H_{43}N_3O_{11}S$	761.85
a6	DB00872 [B]	Conivaptan	App.; Inv.	$C_{32}H_{26}N_4O_2$	498.59
a7	DB08827 [B]	Lomitapide	App.; Inv.	$C_{39}H_{37}F_6N_3O_2$	693.73
a8	DB01167 [B]	Itraconazole	App.; Inv.	$C_{35}H_{38}Cl_2N_8O_4$	705.63
a9	DB00444 [B]	Teniposide	App.	$C_{32}H_{32}O_{13}S$	656.65
a10	DB00864 [B]	Tacrolimus	App.; Inv.	$C_{44}H_{69}NO_{12}$	804.02
a11	DB06290 [B]	Simeprevir	App.	$C_{38}H_{47}N_5O_7S_2$	749.94
a12	DB00549 [B]	Zafirlukast	App.; Inv.	$C_{31}H_{33}N_3O_6S$	575.68
a13	DB00646 [B]	Nystatin	App; App^{V}	$C_{47}H_{75}NO_{17}$	926.09
b1	DB04868 [B]	Nilotinib	App.; Inv.	$C_{28}H_{22}F_3N_7O$	529.51
b2	DB00390 [B]	Digoxin	App.	$C_{41}H_{64}O_{14}$	780.94
b3	DB13879 [B]	Glecaprevir	App.; Inv.	$C_{38}H_{46}F_4N_6O_9S$	838.87
b4	DB09158 [B]	Trypan blue	App.	$C_{34}H_{28}N_6O_{14}S_4$	872.87
b5	DB09534 [B]	Ecamsule	App.	$C_{28}H_{34}O_8S_2$	562.69
b6	DB00762 [B]	Irinotecan	App.; Inv.	$C_{33}H_{38}N_4O_6$	586.68
b7	DB06809 [B]	Plerixafor	App.	$C_{28}H_{54}N_8$	502.78
b8	DB11581 [B]	Venetoclax	App.; Inv.	$C_{45}H_{50}ClN_7O_7S$	868.45
c1	DB09297 [B]	Paritaprevir	App.; Inv.	$C_{40}H_{43}N_7O_7S$	765.886
c2	DB01248 [B]	Docetaxel	App.; Inv.	$C_{43}H_{53}NO_{14}$	807.89
c3	DB01201 [B]	Rifapentine	App.; Inv.	$C_{47}H_{64}N_4O_{12}$	877.03
c4	DB00877 [B]	Sirolimus	App.; Inv.	$C_{51}H_{79}NO_{13}$	914.19
c5	DB01590 [B]	Everolimus	App.	$C_{53}H_{83}NO_{14}$	958.24
c6	DB00615 [B]	Rifabutin	App.; Inv.	$C_{46}H_{62}N_4O_{11}$	847.00
c7	DB06772 [B]	Cabazitaxel	App.	$C_{45}H_{57}NO_{14}$	835.93
c8	DB00320 [B]	Dihydro-ergotamine	App.; Inv.	$C_{33}H_{37}N_5O_5$	583.67
c9	DB00696 [B]	Ergotamine	App.	$C_{33}H_{35}N_5O_5$	581.66

ID, Identification; [A], ID from Zinc15;[8] [B], ID from Drugbank;[32] App, approved; Inv. Investigational; App^{V}, vet approved; [C], ID from PubChem;[33] MW, Molecular Weight.

AUDs Alcohol use disorders
AMs Allosteric modulators
NAMs Negative allosteric modulators
PAMs Positive allosteric modulators

Supplementary Materials

Supplementary materials can be found at www.mdpi.com/xxx/s1.

Author Contributions

Acquisition of funds, revision and edition, G.R. and M.G.N.-P.; Methodology and Software, F.R.-E.; E.L.-G; Validation and Data curation, F.R.-E. and V.B.-G.; Formal Analysis and Drafting of the initial draft, F. R.-E. and G.R.

Appendix A

The sequence alignment of the four organisms involved (*H. sapiens*, Q99571; *R. norvegicus*, P51577; *M. musculus*, Q9JJX6; and *D. rerio*, Q6NYR1 organisms) is presented in Figure A1.

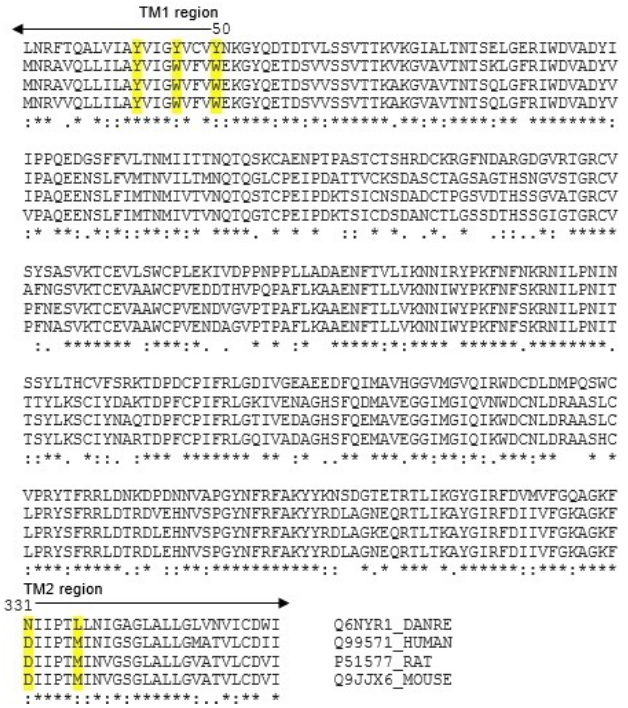

Figure A1. Multiple sequence alignment of the constructed molecular models. Alignments were executed with the Crustal Omega tool.[42–43]

A 3D alignment was also made; the models built by homology were aligned on their respective PDBs used as a template. These results are presented in Figure A2.

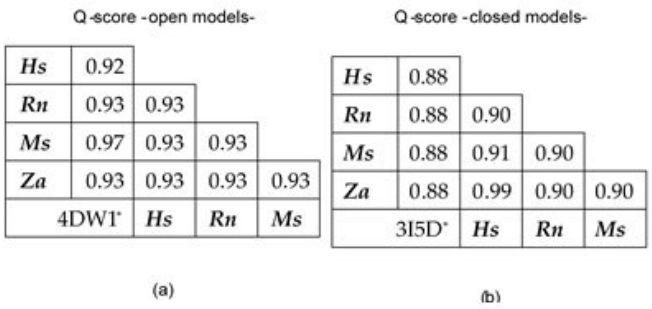

Figure A2. Multiple alignment 3D results obtained with PDBeFOLD program.[44] Q-score, Cα-alignment; *, PDB template; Hs, *H. sapiens*; Rn, *R. norvegicus*; Ms, *M. musculus*; Za, *D. rerio*.

In order to show an example of characteristic potential binding pockets on the 3D structure of P2X4Rs, the structure PDB 3I5D was evaluated with the DoGSiteScorer program.[24] The global properties show different properties in the three sites identified in the TM region (Figure A3). In order to perform molecular docking, the study was carried out considering the cavity with the highest drug score registered in the P2X4Rs models constructed by homology.

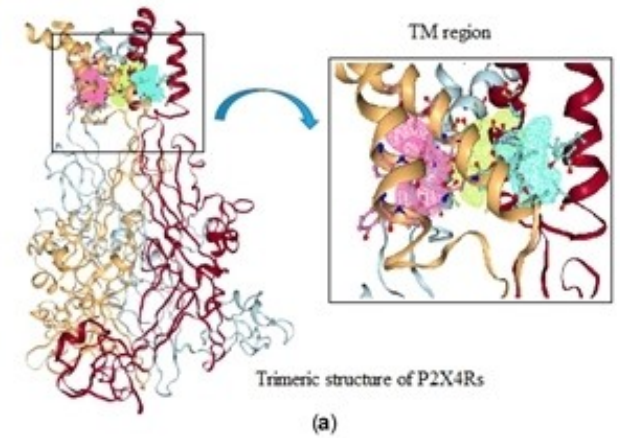

Table A1 Results (DoGSiteScorer).

Site	Volume Å	Surface Å	Drug score
A	278.47	534.72	0.57
B	187.17	360.33	0.52
C	158.62	335.55	0.34

(b)

Figure A3. Prediction of (sub)pockets near TM region on P2X4Rs. (a) 3D representation of PDB 3I5D; In box show binding site detection performed by DoGSiteScore program:[24] site A in cyan, site B in magenta and site C in green. (b) Global properties.

Appendix B

The 2D structures of the molecules recorded in the docking analysis are presented in Table B1. The 2D graphic representation of the molecules was generated with the MarvinSketch program.[45]

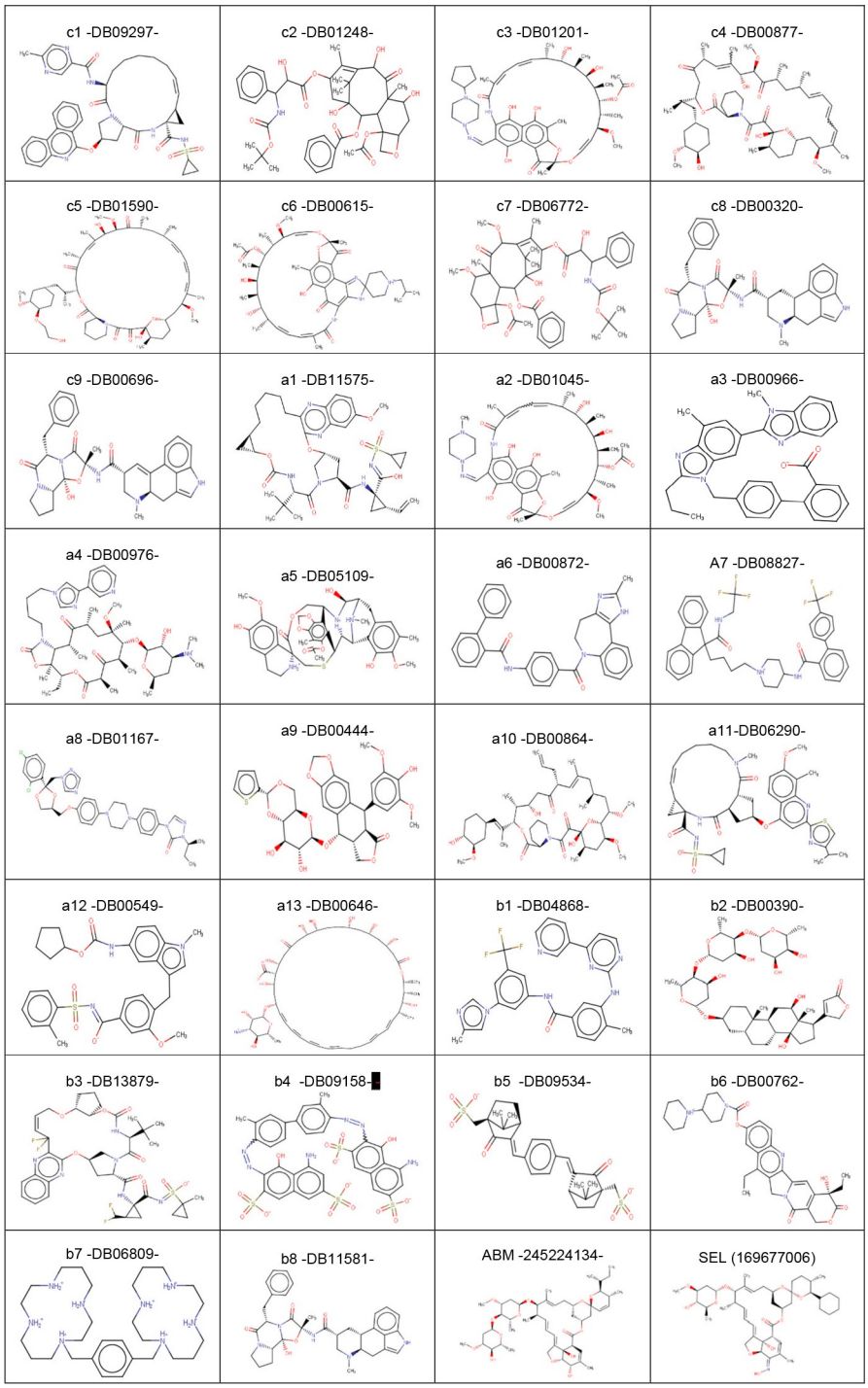

Table B1. 2D molecules structures of data Table 3.

Acknowledgments

This work was supported by the National Council of Science and Technology (CONACyT, México) by grant number Postdoc, CVU 204984 to F.R.E.

Conflict of Interest

None declared.

References

[1] National Institute on Alcohol Abuse and Alcoholism (NIAAA). Available online: https://www.niaaa.nih.gov/alcohol-health/overview-alcohol-consumption/alcohol-use-disorders (accessed 1 March 2019).
[2] B. S. Khakh, W. R. Proctor, T. V. Dunwiddie, C. Labarca, H. A. Lester, *J. Neurosci.* **1999**, *19*, 7289–7299.
[3] L. Asatryan, M. Popova, D. Perkins, J. R. Trudell, R. L. Alkana, D. L. Davies, *J. Pharmacol. Exp. Ther.* **2010**, *334*, 720–728.
[4] V. Latapiat, F. E. Rodríguez, F. Godoy, F. A. Montenegro, N. P. Barrera, J. P. Huidobro-Toro, *Front. Pharmacol.* **2017**, *918*, 1–13.
[5] Y. H. Jo, E. Donier, A. Martinez, M. Garret, E. Toulmé, E. Boué-Grabot, *J. Biol. Chem.* **2011**, *286*, 19993–20004.
[6] J. Suurväli, P. Boudinot, J. Kanellopoulos, S. Rüütel-Boudinot, *Biomed. J.* **2017**, *40*, 245–256.
[7] T. Sterling, J. J. Irwin, *J. Chem. Inf. Model.* **2015**, *55*, 2324–2337.
[8] ZINC15. Available online: http://zinc15.docking.org (accessed on 1 December 2018).
[9] The UniProt Consortium, UniProt: The universal protein knowledgebase. *Nucleic. Acids. Research.* **2017**, 45(D1), D158–D169.
[10] UniProtKB. Available online: http://www.uniprot.org/help/uniprotkb (accessed on 1 February 2019).
[11] A. Waterhouse, M. Bertoni, S. Bienert, G. Studer, G. Tauriello, R. Gumienny, F. T. Heer, T. A. P. de Beer, C. Rempfer, L. Bordoli, R. Lepore, T. Schwede, *Nucleic Acids Res.* **2018**, *46*, W296–W303.
[12] SWISS-MODEL. Available online: https://swissmodel.expasy.org/ (accessed on 1 February 2019).
[13] M. Hattori, E. Gouaux, *Nature* **2012**, *485*, 207–212.
[14] T. Kawate, J. C. W. T. Michel-Birdsong, E. Gouaux, *Nature* **2009**, *460*, 592–598.
[15] H. M. Berman, J. Westbrook, Z. Feng, G. Gilliland, T. N. Bhat, H. Weissig, I. N. Shindyalov, P. E. Bourne, *Nucleic Acids Res.* **2000**, *28*, 235–242.
[16] RCSB PDB. Available online: www.rcsb.org (accessed on 2 February 2019).
[17] E. F. Pettersen, T. D. Goddard, C. C. Huang, G. S. Couch, D. M. Greenblatt, E. C. Meng, T. E. Ferrin, *J. Comput. Chem.* **2004**, *25*, 1605–1612.
[18] G. M. Morris, R. Huey, W. Lindstrom, M. F. Sanner, R. K. Belew, D. S. Goodsell, A. J. Olson, *J. Comput. Chem.* **2009**, *16*, 2785–91.
[19] O. Trott, A. J. Olson, *J. Comput. Chem.* **2010**, *31*, 455–461.
[20] S. Salentin, S. Schreiber, V. J. Haupt, M. F. Adasme, M. Schroeder, *Nucleic Acids Res.* **2015**, *43*, W443–W447.
[21] PLIP. Available online: http://plip.biotec.tu-dresden.de/plip-web (accessed on 1 March 2019).
[22] F. Reyes-Espinosa, A. Juárez-Saldivar, C. García-Pérez, I. Palos, V. Herrera-Mayorga, G. Rivera, *Int. J. Mol. Sci.* **2019**, *20*, 1320.
[23] A. Volkamer, D. Kuhn, T. Grombacher, F. Rippmann, M. Rarey, *J. Chem. Inf. Model.* **2012**, *52*, 360–372.
[24] M. Popova, L. Asatryan, O. Ostrovskaya, L. R. Wyatt, K. Li, R. L. Alkana, D. L. Davies, *J. Neurochem.* **2010**, *112*, 307–317.
[25] K. M. Franklin, L. Asatryan, M. W. Jakowec, *Front. Neurosci.* **2014**, *8*, 176.
[26] R. Prichard, C. Ménez, A. Lespine, *Int. J. Parasitol. Drug. Resist.* **2012**, *2*, 134–153.
[27] L. Asatryan, M. M. Yardley, S. Khoja, J. R. Trudell, N. Hyunh, S. G. Louie, N. A. Petasis, R. L. Alkana, D. L. Davies, *Int. J. Neuropsychopharmacol.* **2014**, *17*, 907–916.
[28] S. Khoja, N. Huynh, A. M. P. Warnecke, L. Asatryan, M. W. Jakowec, D. L. Davies, *Psychopharmacology* **2018**, *235*, 1697–1709.
[29] T. Sander, J. Freyss, M. von Korff, C. Rufener, *J. Chem. Inf. Model.* **2015**, *55*, 460–73.
[30] A. Zabala, N. Vazquez-Villoldo, B. Rissiek, J. Gejo, A. Martin, A. Palomino, A. Perez-Samartín, K. R. Pulagam, M. Lukowiak, E. Capetillo-Zarate, J. Llop, T. Magnus, F. Koch-Nolte, F. Rassendren, C. Matute, M. Domercq, *EMBO Mol. Med.* **2018**, *10*, 1–20.
[31] F. Di Virgilio, A. C. Sarti, *EMBO Mol. Med.* **2018**, *10*, 1–3.
[32] DrugBank. Available online: https://www.drugbank.ca/ (Accessed 1 Marc 2019).
[33] Pubchem. Available online: https://pubchem.ncbi.nlm.nih.gov/ (Accessed 1 Marc 2019).
[34] A. Abdelrahman, V. Namasivayam, S. Hinz, A. C. Schiedel, M. Köse, M. Burton, A. El-Tayeb, M. Gillard, J. M. Bajorathde Ryck, C. E. Müller, *Biochem. Pharmacol.* **2017**, *125*, 41–54.
[35] J. Sandkühler, *Physiol. Rev.* **2009**, *89*, 707–758.
[36] A. Franceschini, E. Adinolfi, *World J. Biol. Chem.* **2014**, *5*, 429–436.
[37] F. Li, N. Guo, Y. Ma, B. Ning, Y. Wang, L. Kou, *Inflammation* **2014**, *37*, 146–153.
[38] H. Chen, Q. Xia, X. Feng, F. Cao, H. Yu, Y. Song, X. Ni, *Mol. Med. Rep.* **2016**, *13*, 697–704.
[39] G. Burnstock, *Adv. Pharmacol.* **2016**, *75*, 91–137.
[40] L. Chen, Y. W. Liu, K. Yue, Q. Ru, Q. Xiong, B. M. Ma, X. Tian, C. Y. Li, *Purinergic. Signal.* **2016**, *12*, 79–87.
[41] L. Wang, X. Feng, B. Hu, Q. Xia, X. Ni, Y. Song, *Purinergic. Signal.* **2018**, *14*, 433–442.
[42] F. Sievers, D. G. Higgins, *Clustal omega. Curr. Prot. Bioinform.* **2014**, *48*, 3.13.1–3.13.16.
[43] Multiple Sequence Alignment. Clustal Omega. Available online: https://www.ebi.ac.uk/Tools/msa/clustalo/ (accessed on 25 Jan 2020).
[44] E. Krissinel, K. Henrick, *Acta Crystallogr.* **2004**, *D60*, 2256–2268.
[45] Marvin was used for drawing, displaying and characterizing chemical structures, substructures and reactions, Marvin 17.22.0, 2017, ChemAxon. Available online: http://www.chemaxon.com. (Accessed 1 December 2018.

Received: August 19, 2019
Accepted: April 22, 2020
Published online on June 8, 2020

